Dynamics of the connectome in Huntington's disease: A longitudinal diffusion MRI study

Omar F.F. Odish[a,*,1], Karen Caeyenberghs[b,1], Hadi Hosseini[c], Simon J.A. van den Bogaard[a], Raymund A.C. Roos[a], Alexander Leemans[d]

[a]Department of Neurology, Leiden University Medical Center, Leiden, The Netherlands
[b]Faculty of Health Sciences, School of Psychology, Australian Catholic University, Melbourne, Australia
[c]Department of Psychiatry and Behavioral Sciences, School of Medicine, Stanford University, Stanford, CA, USA
[d]Image Sciences Institute, University Medical Center Utrecht, Utrecht, The Netherlands

ARTICLE INFO

ABSTRACT

Objectives: To longitudinally investigate the connectome in different stages of Huntington's disease (HD) by applying graph theoretical analysis to diffusion MRI data.
Experimental design: We constructed weighted structural networks and calculated their topological properties. Twenty-two premanifest (preHD), 10 early manifest HD and 24 healthy controls completed baseline and 2 year follow-up scans. We stratified the preHD group based on their predicted years to disease onset into a far (preHD-A) and near (preHD-B) to disease onset group. We collected clinical and behavioural measures per assessment time point.
Principle observations: We found a significant reduction over time in nodal betweenness centrality both in the early manifest HD and preHD-B groups as compared to the preHD-A and control groups, suggesting a decrease of importance of specific nodes to overall network organization in these groups (FDR adjusted $ps < 0.05$). Additionally, we found a significant longitudinal decrease of the clustering coefficient in preHD when compared to healthy controls (FDR adjusted $p < 0.05$), which can be interpreted as a reduced capacity for internodal information processing at the local level. Furthermore, we demonstrated dynamic changes to hub-status loss and gain both in preHD and early manifest HD. Finally, we found significant cross-sectional as well as longitudinal relationships between graph metrics and clinical and neurocognitive measures.
Conclusions: This study demonstrates divergent longitudinal changes to the connectome in (pre) HD compared to healthy controls. This provides novel insights into structural correlates associated with clinical and cognitive functions in HD and possible compensatory mechanisms at play in preHD.

1. Introduction

Recent years have seen an increase in work pertained to finding and developing biomarkers for Huntington's disease (HD) and its premanifest stage (preHD). HD is an autosomal dominant neurodegenerative disorder caused by an elongated cytosine–adenine–guanine (CAG) repeat on the short arm of chromosome 4, which leads to the production of mutated huntingtin protein [1]. Prominent white and grey matter atrophy appear in the course of the disease [2–5]. This results in cognitive deterioration, including slower processing speed, attentional problems, executive control deficits and ultimately dementia, but also motor signs such as chorea, bradykinesia, rigidity and dystonia and psychiatric symptoms such as depression, anxiety and apathy.

Finding biomarkers that assess progression towards disease manifestation and follow disease advancement at the clinical stage, is of importance in the light of understanding the impact of intervention trials. One of the most promising methods currently being deployed to probe for biomarker potential is diffusion MRI, which can characterize tissue microstructure via the diffusion of water molecules [6–9]. Based on this technique, several cross-sectional studies in HD have provided evidence for abnormal structural organization of the brain, typically using region of interest and tract-based spatial statistics analyses [10–14]. However, findings from longitudinal reports using diffusion MRI in HD remain inconsistent [15–17].

In the study by Weaver et al. [16], the tract-based spatial statistics approach was used to compare scans from seven controls, four preHD and three manifest HD subjects obtained 1 year apart. Significant

---

longitudinal decreases in white matter fractional anisotropy and axial diffusivity in the seven (pre)manifest subjects were found compared to the healthy controls. In another study by Sritharan et al. [17] with 17 controls and 18 manifest HD subjects, a region of interest approach did not reveal longitudinal changes in the mean diffusivity of the caudate, putamen, thalamus and corpus callosum over a 1 year period, while baseline mean diffusivity was found to be significantly higher in the caudate and putamen of subjects with manifest HD compared to controls. A similar finding for mean diffusivity was reported by Vandenberghe et al. [15] in eight manifest HD subjects over a 2 year period, also using a region of interest approach. These inconsistencies in the literature might very well be attributed to inconsistencies in defining the regions of interest or to other methodological limitations, such as those recently described for tract-based spatial statistics [18]. As longitudinal sensitivity to detecting disease progression is an essential quality of a biomarker, and given the abovementioned apparent lack of uniformity in previous longitudinal reports, we used a graph theoretical approach to analyse our data from a new perspective.

A graph theoretical analysis (GTA) is a powerful mathematical framework for quantifying topological properties of networks. This type of analysis moves away from the traditional neuroimaging approach of examining individual components of the brain, such as regions of interest, towards characterizing regional or global structure of networks. In recent years, this paradigm shift from segregation to integration has emerged as a useful strategy for characterizing functional and structural brain networks in healthy and clinical groups, including other neurodegenerative diseases such as Alzheimer's disease [19–23], neuroimmunological disorders such as multiple sclerosis [24,25], but also in traumatic brain injury [26,27] and schizophrenia [28,29]. Using network based statistics, one recent *cross-sectional* study by Poudel et al. [30] provided evidence for aberrant white matter cortico-striatal connectivity in HD compared to controls based on diffusion MRI data. However, little research has been done on the dynamics of structural brain networks using a *longitudinal* design.

GTA may provide more insights into structural changes that can develop over the course of the condition, which may be too subtle to be detected at the local level. We therefore investigated network dynamics of the connectome in individuals from a well-defined cohort (TRACK-HD study [31]) assessed systematically and prospectively across multiple time points. This could provide new insights into the development of topological organization of whole-brain structural connectivity in HD, possibly providing usable markers quantifying disease progression. Such biomarkers can potentially be used, in turn, as targets for modification in therapeutic trial settings, especially in the premanifest phase where the priority lies in preventing or delaying manifestation of this devastating disorder. It is also important to examine potential associations between currently used cognitive and clinical measures in HD and (disrupted) network properties, thereby providing a more tangible 'real-world' sense to the complexity of brain structure and function.

2. Materials and methods

2.1. Participants

As part of the TRACK-HD study, 90 participants were included at baseline at the Leiden University Medical Center (LUMC) study site. Recruitment procedures and inclusion criteria have been published previously (for details see [2]). Diffusion MRI was added to the standard MRI protocol. At baseline, diffusion MRI was not performed in ten participants because of claustrophobia, and another nine were excluded from analysis due to excessive motion artefacts, which caused significant data corruptions, such as large signal dropouts and intra-volume inter-slice distortions. Such corrupted data sets were deemed unusable for inclusion in the study and were therefore not considered for further processing and analysis. Of the remaining 71 subjects, 62 subjects completed diffusion MRI scans at both visits with an average between-scan

interval of 23 months. Of these 62, a further six subjects were excluded from analysis due to excessive motion artefacts at the second visit. The longitudinal cohort included in this work was thus comprised of 56 subjects: 24 healthy controls, 22 preHD and 10 early manifest HD subjects (Table 1).

Inclusion criteria for the preHD group were a CAG repeat ≥40 with a total motor score on the Unified Huntington's Disease Rating Scale (UHDRS-TMS) ≤ five [2]. Moreover, to assess the effect of expected proximity to disease onset on diffusion parameters, the preHD group was divided at baseline according to the median (10.9 years) for the predicted years to disease onset into preHD-A (≥10.9 years) and preHD-B (<10.9). The predicted years to disease onset was based on a formula by Langbehn et al. [32] using CAG repeat length and age-based survival analysis. This resulted in two groups (preHD-A and preHD-B) each consisting of 11 subjects (Table 1). Inclusion criteria for the early manifest HD group were a CAG repeat ≥40, with a UHDRS-TMS ≥five and a Total Functional Capacity score (TFC) ≥seven. For both the preHD and early manifest HD groups, a burden of pathology score greater than 250 ((CAG repeat length − 35.5) × age) was applied as a further inclusion criterion [2,33]. Healthy gene negative family members or partners were recruited as control subjects. None of the participants suffered from a concomitant neurological disorder, a major psychiatric diagnosis, or had a history of severe head injury.

Demographics, clinical information, and neurocognitive measures of interest are provided in Table 1. From the neurocognitive battery administered, the Stroop Word Reading (SWR) task and the Trail Making Task (TMT) were chosen as measures of interest, as these tasks have shown promising results as cognitive disease-state markers in HD research [31,34,35]. In short, the SWR task consisted of the instruction of reading a set of words of colours (red, green and blue) as fast as possible within 45 s. The number of correct responses was computed using the number of items completed, with higher scores reflecting faster processing speed. The SWR has been used as a sensitive outcome measure in studies identifying predictors of longitudinal decline in HD, independent of disease related motor effects [31]. Furthermore, the TMT was administered which requires inhibition, updating, and switching, and consists of two parts, Trails A and Trails B. In Trails A, letters from A to Y are distributed across the page and participants are asked to draw lines connecting the letters from the alphabet in the right order, without lifting the pencil from the page. In Trails B, the page contains the numbers from 1 to 12 and letters from A to L and participants must connect the symbols by alternating the sequence between numbers and letters, that is, A-1-B-2-C-3… L-12. The dependent variable was the switch cost calculated by subtracting time to complete part A from part B. The validated Dutch version of the National Adult Reading Test (DART) was used to assess the intelligence quotient [36]. Finally, the Beck Depression Inventory-II (BDI-II) was administered, which is a 21-question multiple-choice self-report inventory, one of the most widely used instruments for measuring severity of depression. All participants completed both baseline as well as follow-up MRI, cognitive and clinical evaluation. The study was approved by the Medical Ethics Committee of the LUMC and written informed consent was obtained from all participants.

2.2. MRI acquisition

MRI acquisition was performed with a 3-Tesla whole-body scanner (Philips Achieva, Healthcare, Best, The Netherlands) using an eight channel SENSE head coil. T1-weighted image volumes were acquired using a 3D MPRAGE acquisition sequence with the following imaging parameters: TR = 7.7 ms, TE = 3.5 ms, FOV = 24×24 cm^2, matrix size 224×224, number of slices = 164, slice thickness = 1.00 mm, and no slice gap. A single-shot echo-planar diffusion tensor imaging sequence was applied with 32 measurement directions and the following scan parameters [8]: TR = 10,004 ms, TE = 56 ms, FOV = 220×220 mm^2 with an acquisition matrix of 112×110, 2.00 mm

Table 1
Group demographics with clinical and behavioural scores.

		Healthy controls	Premanifest HD (A and B)	preHD-A	preHD-B	Early manifest HD
N		24	22[e]	11	11	10
Gender male/female		11/13	9/13	4/7	5/6	4/6
Age in years (at V1), mean (SD)		49.0 (8.2)	43.6 (8.7)	44.2 (5.7)	43.0 (11.2)	50.2 (9.3)
Handedness R/L		20/4	18/4	9/2	9/2	9/1
Level of education (ISCED), median (range)		4 (3)	4 (3)	4 (3)	4 (3)	4 (3)
DART-IQ, mean (SD)		105.0 (9.4)	100.5 (11.2)	101.3 (9.7)	99.6 (13.0)	101.8 (13.5)
CAG repeat length, mean (SD)		n/a	42.6 (2.7)	41.3 (1.4)	43.9 (3.1)[d]	42.5 (1.2)
Estimated years to onset, mean (SD)		n/a	11.8 (4.7)	14.9 (4.7)	8.6 (1.8)[d]	n/a
Total functional capacity, mean (SD)	V1	13.0 (0.2)	12.8 (0.5)	12.7 (0.7)	12.8 (0.4)	11.0 (1.5)[b]
	V2	12.9 (0.5)	12.6 (0.9)	12.7 (0.6)	12.5 (1.0)	10.3 (2.2)[b]
UHDRS-TMS, mean (SD)	V1	2.6 (2.5)	2.6 (1.5)	2.0 (1.5)	3.1 (1.2)	14.6 (7.7)[b]
	V2	2.1 (1.6)	5.7 (5.1)[c]	3.5 (2.2)	8.3 (6.1)[a,d]	23.0 (12.1)[b]
SWR, mean (SD)	V1	100.1 (13.2)	91.9 (14.2)[a]	95.6 (9.6)	88.3 (17.3)[a]	87.7 (14.7)[a]
	V2	102.0 (15.6)	87.9 (15.7)[a]	91.4 (9.4)	84.4 (20.0)[a]	86.4 (18.6)[a]
Switch cost of TMT in seconds, mean (SD)	V1	37.0 (17.4)	41.8 (24.6)	36.4 (15.9)	47.2 (30.9)	63.5 (41.6)[b]
	V2	38.9 (27.0)	38.0 (28.6)	30.8 (19.2)	45.8 (35.7)	75.0 (63.4)[b]
BDI-II, mean (SD)	V1	4.1 (4.4)	6.4 (6.4)	4.9 (6.0)	7.9 (6.8)	10.2 (8.2)[a]
	V2	3.9 (4.1)	5.1 (5.6)	3.2 (4.9)	6.9 (5.9)	8.2 (8.4)
Between-scan interval in months, mean (SD)		23.0 (0.8)	23.0 (0.7)	23.2 (0.6)	22.7 (0.7)	23.5 (0.7)

HD = Huntington's disease, N = number of participants, SD = standard deviation, n/a = not applicable, ISCED = International Standard Classification of Education, DART-IQ = Dutch Adult Reading Test Intelligence Quotient, CAG = cytosine–adenine–guanine, UHDRS-TMS = Unified Huntington's Disease Rating Scale-Total Motor Score, SWR = Stroop Word Reading task, TMT = Trail Making Task, BDI-II = Beck Depression Inventory-II, V1 = visit 1, V2 = visit 2.
Significance at $p \leq 0.05$ level:
[a] Significantly different from controls.
[b] Significantly different from controls and premanifest HD.
[c] Significantly different from controls and early manifest HD.
[d] Significantly different from preHD-A.
[e] Including five subjects progressing to the early manifest stage during the 2 year follow-up period.

slice thickness, transversal slice orientation, no slice gap, flip angle = 90°, reconstruction voxel dimensions of $1.96 \times 1.96 \times 2.00$ mm^3, number of slices = 64, b-value = 1000 s/mm^2, half-scan factor = 0.61. Parallel imaging (SENSE) was used with a reduction factor of two, NSA = one, and fat suppression was applied. Diffusion MRI acquisition time was 6.55 min.

2.3. Diffusion MRI processing

Diffusion MRI data were analysed using the diffusion MR toolbox 'ExploreDTI' [37]. Data were corrected for subject motion, eddy current distortions, and susceptibility artefacts due to the magnetic field inhomogeneity prior to diffusion tensor estimation with the REKINDLE method [37–40]. Whole-brain fibre tractography was performed using constrained spherical deconvolution [41–43] with a uniform seed point resolution of 2 mm^3, an angle threshold of 30°, a fibre orientation distribution threshold of 0.1, and maximum harmonic order of 4.

2.4. Connectivity matrices

One structural network was generated for each subject using the subject's diffusion MRI data. A network was defined as a set of nodes (denoting anatomical regions of the parcellation scheme) and interconnecting edges (denoting fibre trajectories between the cortical and subcortical regional nodes that have been reconstructed). Moreover, we assigned a continuous weight (i.e., number of streamlines) to each edge of the graph, which resulted in weighted graphs. Because tractography does not differentiate between efferent and afferent fibres, the reconstructed graphs were all undirected. We describe here some of the major steps that we went through from diffusion MRI processing to computing the topological metrics of the graph. Fig. 1 shows a flowchart for the process of obtaining connectivity matrices. The Automated Anatomical Labelling (AAL) atlas (and labels/masks [44]) was registered to the diffusion MRI data using a non-linear transformation [45] with fractional anisotropy as target image contrast [46]. The AAL atlas regions, which are commonly used to derive the nodes in GTA of neuroimaging

data, are presented in Fig. 2. The AAL template is not a pure cortical grey matter mask but includes tissues from both cortical grey matter and subcortical white matter [44,47]. Defining seed voxels throughout the brain parenchyma ensures that the computed trajectories originated from the white matter tissue underlying the cortical region or adjacent to subcortical structures. The average percentage of network tracts connecting a pair of regions was 2.39×10^{-4}. The numbers of streamlines connecting each pair of AAL regions were aggregated into a 90×90 connectivity matrix (the cerebellar regions were not included). We refer the interested reader to the Supplementary video for a three-dimensional example of a resulting connectome.

2.5. Graph theory metrics

We used the Brain Connectivity Toolbox (BCT) ([48]: https://sites.google.com/site/bctnet/) and the longitudinal plugin of the Graph Analysis Toolbox [49–51], to investigate network metrics of segregation, integration, and centrality. Network measures were computed over a range of density thresholds. Thresholding at an absolute value would have resulted in networks with different degrees across groups, introducing a confound when comparing measures between groups [52]. Network measures were examined over a range of network densities for which the networks were not fragmented (each node had at least one connection with another node in the graph) and displayed small-world properties (non-random graphs) [51]. The network densities ranging from 0.10 to 0.40 fulfilled these criteria. We compared the networks in this density range in steps of 0.05. The graph metrics were quantified at both the network and regional levels from the weighted networks. The equations to calculate each of these measures can be found in Rubinov and Sporns [48] (https://sites.google.com/site/bctnet/measures/list). We only provide brief explanations for each of the network properties used in this study.

We quantified measures of network integration (characteristic path length) and segregation (clustering) for each network [48]. The characteristic path length L of a network is the average shortest path
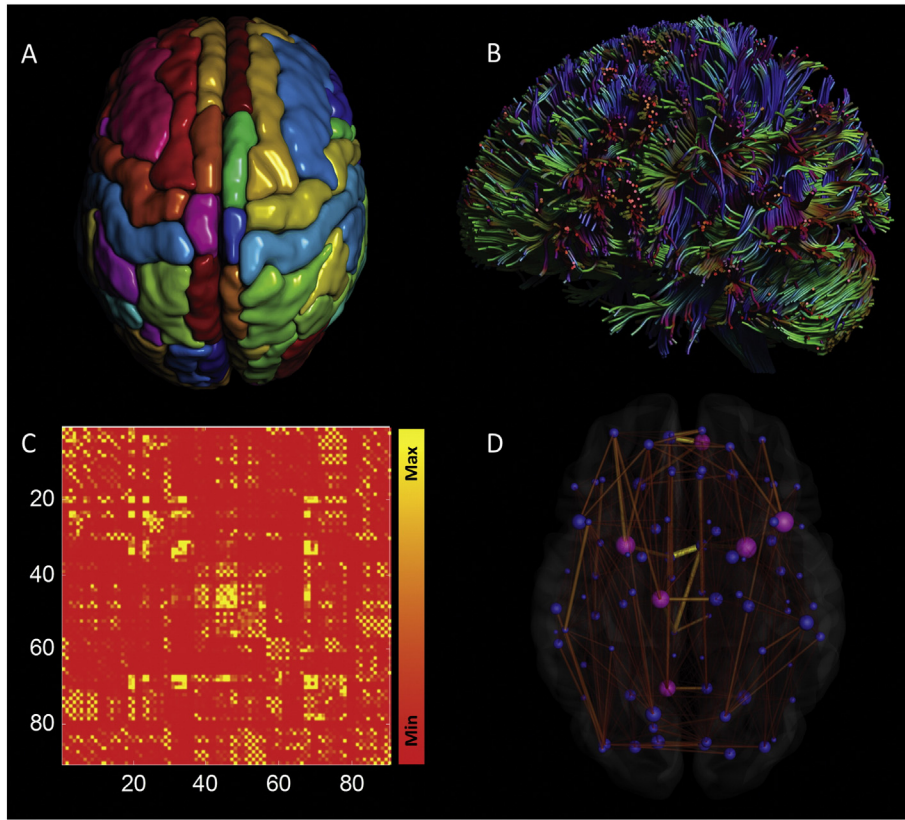
Fig. 1. Flow chart for constructing a diffusion MRI based network. (A) An automated anatomical labeling (AAL) atlas template consisting of 90 cortical and subcortical brain regions, excluding the cerebellum, was used for brain segmentation. (B) Whole brain tractography was performed using ExploreDTI (see the Materials and methods section). (C) The numbers of streamlines connecting each pair of AAL regions were aggregated into a 90 × 90 weighted connectivity matrix. (D) The connectivity matrix was then visualized as a graph, composed of nodes representing brain regions and edges representing white matter connections. From the individual weighted brain networks, several network metrics were computed at both the global and regional levels.

(distance) between all pairs of nodes in the network. It is defined as:

$$L = \frac{1}{n} \sum_{i \in N} \frac{\Sigma_{j \in N, j \neq i} d_{ij}}{n-1}$$

where d_{ij} is the shortest path length (distance) between nodes i and j. The global efficiency [53] is the average inverse shortest path length in the network, and is inversely related to the characteristic path length. In other words, networks with a small average characteristic path length are generally more efficient than those with large average characteristic path length. We also calculated local efficiency as a nodal graph metric. The regional efficiency is the global efficiency computed on node neighbourhoods [54], and is related to the clustering coefficient.

The clustering coefficient of a node is a measure of the number of edges that exist between its nearest neighbours and is quantified by counting the numbers of triangles formed around a node [55,56]. The clustering coefficient C of het network is the average clustering across all nodes and is quantified as:

$$C = \frac{1}{n} \sum_{i \in N} \frac{2t_i}{k_i(k_i-1)}$$

where k_i is the number of connections (degree) for node i and ti is the number of triangles around a node i. The modularity is a graph metric that quantifies the degree to which the network may be subdivided into clearly delineated nonoverlapping groups of nodes in a way that maximizes the number of within-group edges, and minimizes the number of between-group edges. To evaluate the topology of the

constructed networks, the obtained characteristic path length and clustering coefficient of each network were normalized to the corresponding mean values of null networks with the same degree-, weight- and strength-distributions as the network of interest [57,58], using the null model algorithm implemented in BCT [48].

We also computed the small-world index as the ratio of normalized clustering and normalized path length [59,60]. Thus, the small-worldness index of each network was obtained as $[C/C_{rand}]/[L/L_{rand}]$, where C_{rand} and L_{rand} are the mean clustering coefficient and the characteristic path length of random networks [61]. In a small-world network, the clustering coefficient is significantly higher than that of random networks (C/C_{rand} ratio greater than 1), while the characteristic path length is comparable to random networks (L/L_{rand} ratio close to 1).

Finally, we have calculated node betweenness centrality [62], which is the fraction of all shortest paths in the network that contain a given node. The betweenness centrality b_i of a node i is defined as:

$$b_i = \frac{1}{(N-1)(N-2)} \sum_{\substack{h, j \in G \\ h \neq j, h \neq i, j \neq i}} \frac{\rho_{hj(i)}}{\rho_{hj}}$$

in which ρ_{hj} is the number of shortest paths between nodes h and j and $\rho_{hj(i)}$ is the number of shortest paths between nodes h and j that pass through node i. The nodes with the largest betweenness centrality can be considered to be pivotal nodes (i.e., hubs) in the network.

2.6. Statistical analysis

Interaction effects between group and time for the graph metrics were analysed using the Longitudinal plugin of the Graph Analysis
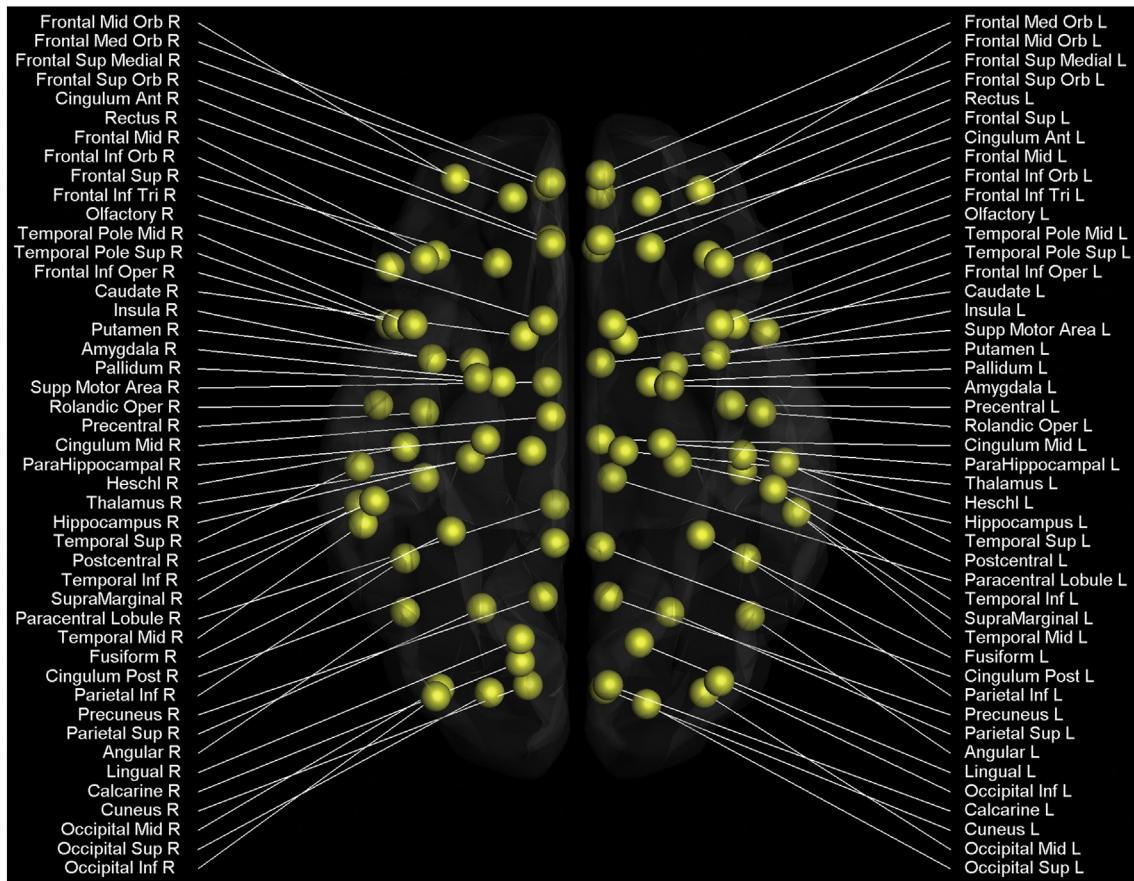
Fig. 2. Cortical and subcortical regions (45 in each hemisphere; 90 in total) as anatomically defined by the automated anatomical labeling atlas template image in standard stereotaxic space.

Toolbox [51,63]. Specifically, networks were first normalized by the mean network strength and graph measures were quantified for the normalized networks. A non-parametric permutation test with 1000 repetitions was then used to test the statistical significance of the effects of time course for graph measures [28,49]. In each permutation, the calculated regional streamlines of each participant were randomly assigned to one of the two groups so that each randomized group had the same number of subjects as in the original groups. Finally, the actual difference in the slope between the original groups was compared to the obtained permutation distribution of difference in slope between randomized groups to obtain the *p*-value.

The same permutation procedure was used to test the significance of the differences in regional network measures. In this step, we compared regional network measures for the networks thresholded at minimum density. We obtained false discovery rate (FDR) corrected *p*-values as measures of significance for the regional measures comparisons. In the present study, the *p*-values reported for regional differences between groups are FDR corrected for multiple comparisons (90 comparisons).

Baseline (i.e., visit 1) data of behavioural metrics (i.e., neurocognitive functioning scores) as well as graph metrics were used for cross-sectional analyses. A multivariate analysis of covariance (MANCOVA) was used, whereby statistical differences were assessed on multiple continuous dependent variables (graph metrics, cognitive and clinical variables) by an independent grouping variable (controls, preHD, early manifest HD), while controlling for a third variable (covariate). In the present study, age was added as covariate so that it could reduce error terms and so that the analysis eliminated the covariates' effect on

the relationship between the independent grouping variable and the continuous dependent variables. We further subdivided the preHD group into two subgroups: preHD far from expected disease onset (preHD-A) and preHD close to expected disease onset (preHD-B).

To investigate the neuronal correlates of the behavioural tests, baseline data were analysed. Each participant's score on tests of clinical scales and neurocognitive functioning was correlated with that participant's graph metric (clustering coefficient, global efficiency, betweenness centrality) using partial correlations (age as confounding variable).

Our final aim was to investigate the relationship between changes in graph metrics with changes in behavioural performance. Difference scores for both behavioural performance and graph metrics were calculated as a measure of change by subtracting the visit 1 from the visit 2 scores.

3. Results

3.1. Baseline group comparison of demographic variables and performance in behavioural tests

Participants of the three groups (controls, preHD, early manifest HD) did not differ in terms of gender distribution ($p = 0.93$), handedness ($p = 0.95$), body mass index ($p = 0.64$) or intelligence quotient scores ($p = 0.38$). One-way ANOVAs revealed only a trend towards a difference in age between the groups ($p = 0.06$). Therefore, we included age as covariate in subsequent analyses. See Table 1 for group demographics and clinical and behavioural scores. The groups differed at

baseline in their executive function performance (SWR and the switch cost of the TMT, all $ps < 0.05$). Post hoc Tukey testing showed significant differences between controls and (pre) HD groups.

3.2. Regional graph analyses

Graph metrics were evaluated at the nodal level to identify the nodes in the network that show a significant group by time interaction effect. Multiple testing correction was performed via False Discovery Rate (FDR) [64], where an FDR adjusted p-value < 0.05 was considered significant. The permutation test of the nodal betweenness centrality showed a significant group by time interaction for the left orbitofrontal cortex and left paracentral lobule (adjusted $ps < 0.05$). The post-hoc two-sided Tukey t-test demonstrated a decrease of the betweenness centrality of the left orbitofrontal cortex in the early manifest HD group as compared to the control group ($p < 0.001$), from the first to the second visit. Moreover, preHD-B patients versus controls demonstrated a reduction of betweenness centrality of the left paracentral lobule from visit 1 to visit 2 ($p < 0.001$). Finally, the permutation test of the clustering coefficient revealed a significant group by time interaction for the left medial prefrontal cortex (adjusted $p < 0.05$). The post-hoc two-sided Tukey t-test showed that preHD showed a decrease of the clustering coefficient of the left medial prefrontal cortex compared to the healthy controls from visit 1 to visit 2 ($p = 0.02$).

3.3. Important network regions as defined by hub-status in visits 1 and 2

Betweenness centrality was also used to identify hub regions. In visit 1, the left precuneus was shared by all groups. Generally, a lower number of areas functioned as network hubs in visit 2 and a remarkable change in hub-status was apparent for regions in visit 2 in each group (as shown in Fig. 3). Specifically in the early manifest HD group, the left thalamus and right medial part of the superior frontal gyrus

achieved hub-status in visit 2. Also, many regions lost their hub-status in visit 2 within the early manifest HD group. Such areas included the left superior temporal pole, right lingual gyrus, right calcarine gyrus, and left middle occipital gyrus. The preHD group also showed hub-changes from visit 1 to visit 2, whereby the right medial part of the superior frontal gyrus lost hub-status. One brain region, the right superior parietal gyrus, achieved hub-status in visit 2. Network nodes in the precuneus, superior temporal pole, and putamen were consistently important as hubs throughout visits 1 and 2 in the preHD group.

3.4. Overall dynamics of the structural brain network

Both (pre-) HD and healthy controls showed a small-world organization of the structural brain networks (as shown in Table 2) expressed by a normalized clustering coefficient gamma >1 (mean|SD; preHD: 1.62 | 0.14, early manifest HD: 1.54 | 0.18, healthy participants: 1.62 | 0.15) and lambda ~1 (mean|SD; preHD: 1.06 | 0.01, early manifest HD: 1.06 | 0.02, healthy participants: 1.06 | 0.01). The small-worldness (sigma) calculated from these indices was also larger than 1 (mean|SD; preHD: 1.52 | 0.12, early manifest HD: 1.45 | 0.16, healthy participants: 1.53 | 0.14). Furthermore, looking at the overall organization characteristics of the brain networks of patients, the normalized clustering coefficient gamma did not differ between preHD, early manifest HD, and healthy controls ($p = 0.31$), nor did the overall normalized path length lambda ($p = 0.69$). In summary, preHD and early manifest HD patients displayed gamma and lambda values close to the values of the brain networks of the healthy controls, suggesting an intact overall organization of the structural brain network in these disease stages.

3.5. Between-group differences in baseline graph metrics

Premanifest and early manifest HD patients did not show strong alterations (all $ps > 0.05$) in whole-brain graph metrics (Table 2). The
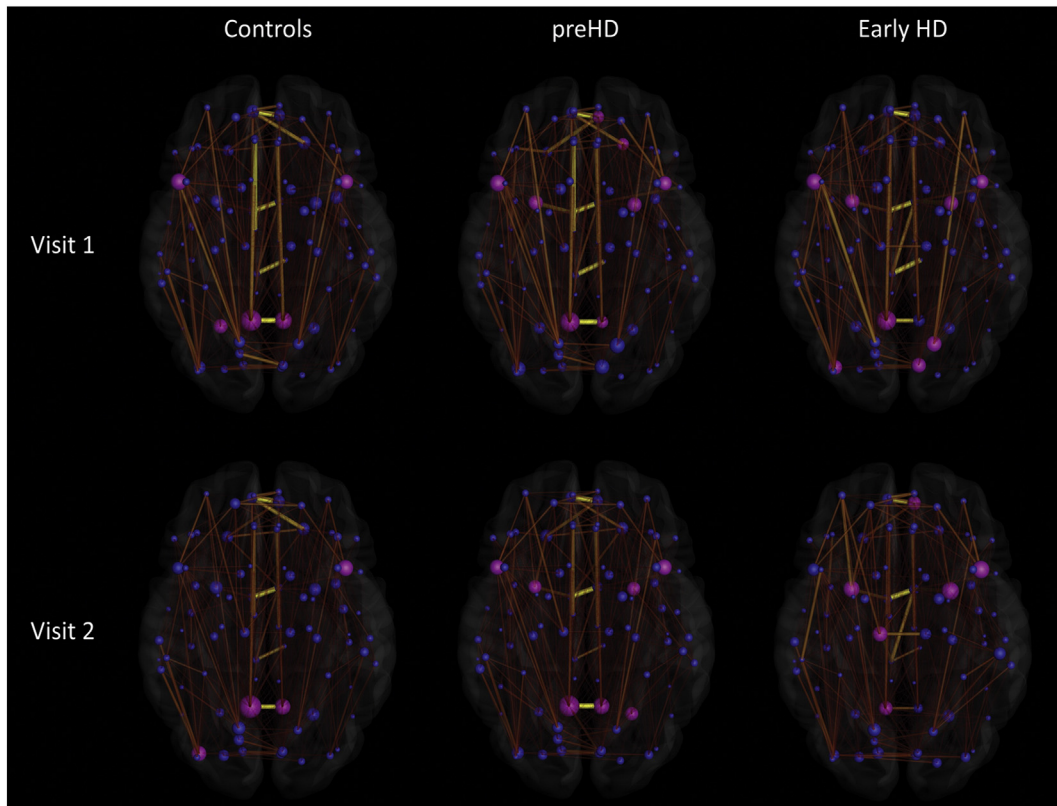

Fig. 3. Group differences in betweenness centrality. Upper panel: visit 1, lower panel: visit 2. Size of the nodes (spheres) represents the betweenness centrality. Size of the edges (connections) represents streamline count. Magenta as color of the nodes refers to hub regions.

Table 2
Graph metrics. Data is shown as mean and standard error of the groups for each visit.

			Healthy controls		Premanifest HD (A and B)		preHD-A		preHD-B		Early manifest HD	
			Mean	SE	Mean	SE	Mean	SE	Mean	SE	Mean	SE
Global network metrics	Global efficiency	V1	0.034	0.0004	0.034	0.0004	0.034	0.0007	0.034	0.0005	0.033	0.0009
		V2	0.035	0.0004	0.034	0.0005	0.034	0.0008	0.034	0.0005	0.033	0.0009
	Characteristic path length	V1	0.110	0.0025	0.111	0.0029	0.112	0.0047	0.109	0.0035	0.107	0.0056
		V2	0.115	0.0027	0.112	0.0033	0.111	0.0056	0.112	0.0036	0.108	0.0057
Small world metrics	Gamma	V1	1.620	0.0309	1.616	0.0307	1.652	0.0413	1.581	0.0448	1.535	0.0578
		V2	1.648	0.0300	1.594	0.0361	1.605	0.0591	1.583	0.0442	1.524	0.0530
	Lambda	V1	1.058	0.0022	1.059	0.0025	1.063	0.0034	1.056	0.0036	1.055	0.0056
		V2	1.057	0.0021	1.056	0.0024	1.055	0.0034	1.057	0.0036	1.053	0.0055
	Sigma	V1	1.530	0.0280	1.525	0.0261	1.553	0.0349	1.496	0.0383	1.453	0.0491
		V2	1.558	0.0266	1.508	0.0316	1.520	0.0517	1.496	0.0387	1.446	0.0433
Local network metrics	Local efficiency	V1	0.051	0.0008	0.051	0.0007	0.051	0.0011	0.050	0.0008	0.049	0.0014
		V2	0.052	0.0007	0.051	0.0008	0.051	0.0014	0.051	0.0010	0.049	0.0015
	Clustering coefficient	V1	0.027	0.0004	0.027	0.0004	0.028	0.0006	0.027	0.0003	0.026	0.0005
		V2	0.027	0.0003	0.027	0.0003	0.027	0.0005	0.027	0.0005	0.026	0.0006
	Modularity	V1	0.319	0.0072	0.315	0.0077	0.326	0.0122	0.304	0.0086	0.291	0.0147
		V2	0.327	0.0063	0.310	0.0091	0.315	0.0141	0.304	0.0120	0.294	0.0129
	Betweenness centrality	V1	90.836	1.0122	91.799	1.1947	92.321	1.8961	91.277	1.5313	89.942	2.5538
		V2	91.835	1.0970	91.100	1.2774	90.806	2.2531	91.394	1.3265	89.436	2.5774

HD = Huntington's disease, V1 = visit 1, V2 = visit 2.

absence of these group effects suggests that global connectivity is relatively intact in early HD.

3.6. Baseline relationships between graph metrics and performance in behavioural benchmark tests

There was a significant negative correlation within the preHD group between baseline individual differences in the switch cost of the TMT on the one hand, and clustering coefficient ($r = -0.44$, $p = 0.05$) and local efficiency ($r = -0.45$, $p = 0.04$), on the other hand (see Fig. 4A and B). Hence, better performance on the TMT (i.e., lower switch cost) was associated with an increase in efficiency and clustering coefficient within the preHD group. Using the subdivision, we found that the switch cost of the TMT was significantly negatively correlated with the local efficiency ($r = -0.69$, $p = 0.03$) and clustering coefficient ($r = -0.78$, $p = 0.008$, survived Bonferroni correction) within the preHD-B group. Moreover, within the preHD-B group, we also observed a positive correlation between the performance on the SWR and global efficiency ($r = 0.62$, $p = 0.05$, Fig. 4C), with higher global efficiency being related to better performance on SWR.

3.7. Baseline relationships between graph metrics and burden

No significant correlations were found between burden and the graph organizational characteristics in the preHD or early manifest HD groups using a Bonferroni correction or even an exploratory uncorrected threshold of $p \leq 0.05$. From this, we cautiously conclude that burden did not explain our findings.

3.8. Longitudinal changes in benchmark behavioural tasks and graph metrics

For the investigation of longitudinal changes on the dependent variables of the behavioural tasks and graph metrics, we subjected each behavioural parameter and graph measure separately to a 2 × 3 permutation test with the between-subject factor group (controls, preHD, early manifest HD) and the within-subject factor time (visit 1, visit 2), while statistically controlling for the effects of age.

We observed a significant group by time interaction effect for the motor score ($F_{(2, 52)} = 17.62$, $p < 0.001$). Post-hoc Tukey t-tests revealed that the early manifest HD group had an increased motor score (i.e., more motor abnormalities) compared to the preHD and healthy control groups. These group differences were even larger on the second

visit ($ps < 0.05$). Also, main effects of the factor group were observed for TFC, SWR, and TMT. The subsequent post-hoc Tukey t-tests indicated generally higher performance for the controls compared to the early manifest HD group across both assessment times ($ps < 0.001$). Furthermore, post-hoc Tukey t-tests showed significantly superior performance on these behavioural tasks for the preHD group compared to the early manifest group ($ps < 0.05$).

The permutation test on modularity showed a significant effect of group, ($F_{(2, 52)} = 3.58$, $p = 0.04$, see Fig. 5A). Across both assessment times, the control group had a larger modularity than the preHD-B and the early manifest HD group ($ps < 0.05$). Furthermore, a trend was observed for the effects of group by time on the normalized clustering coefficient ($p = 0.08$) and small-worldness ($p = 0.06$, Fig. 5B), indicating a trend of increased 'wiring-efficiency' for the control group compared to the (pre) HD groups. Similar results were obtained with the statistical analyses with four groups.

3.9. Correlations between changes in graph metrics and changes in performance on tasks of executive functioning and clinical scales

Partial correlations (with age as confounding variable) between changes in graph metrics from visit 1 to visit 2 in the different groups and the concomitant alterations in the behavioural parameters showed moderate associations between changes in structural network connectivity and the changes in performance on tasks of executive functioning and clinical scales. For the early manifest HD group, there were correlations between the changes in motor score and changes in small-worldness ($r = -0.67$, $p = 0.05$, exploratory threshold, see Fig. 6A). In other words, a decrease in 'wiring-efficiency' was associated with a higher motor score (i.e., more motor symptoms) in the early manifest HD group.

For the combined preHD group, there was a significant negative correlation between normalized path length and scores on BDI-II, pairing more depression symptoms reported with decreased global integration ($r = -0.58$, $p = 0.006$, survived Bonferroni correction, Fig. 6B). For the preHD-B group, correlations were present between changes in scores on the BDI-II and changes in betweenness centrality ($r = -0.80$, $p = 0.006$, survived Bonferroni correction), normalized path length ($r = -0.84$, $p = 0.002$, survived Bonferroni correction), global ($r = -0.64$, $p = 0.05$, exploratory threshold) and local efficiency ($r = -0.66$, $p = 0.04$, exploratory threshold), pairing more symptoms reported on BDI-II with reduced structural connectivity. Furthermore, the difference score of the switch cost of
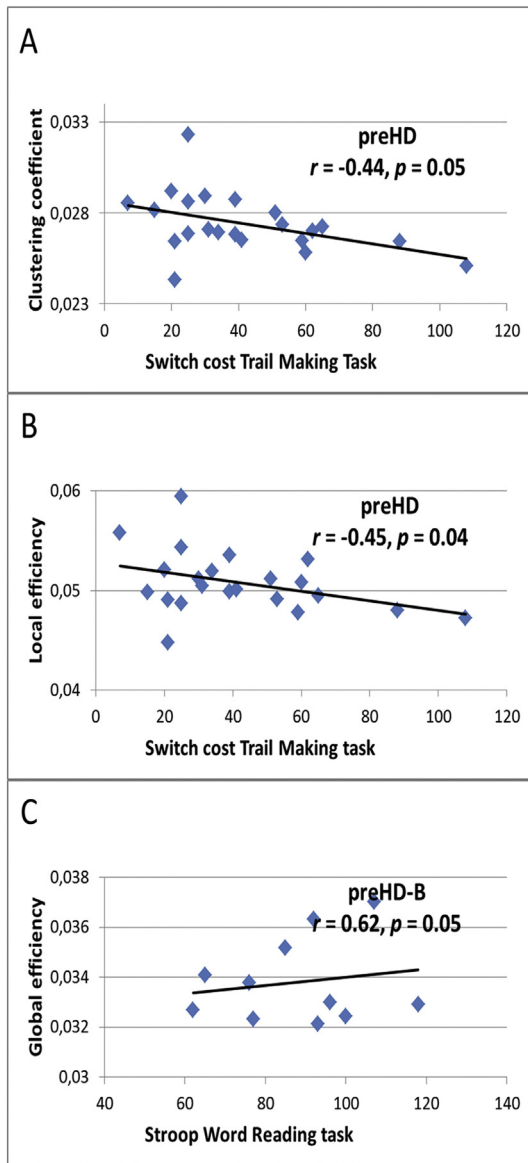
Fig. 4. Baseline correlations between network measures and cognitive performance.

Fig. 5. Longitudinal changes of graph metrics. Visit 1, black bars; visit 2, white bars.

the TMT was significantly negatively correlated with changes in the clustering coefficient ($r = -0.69$, $p = 0.03$, exploratory threshold) within the preHD-B group (Fig. 6C). In other words, an increase in clustering coefficient was associated with better switching performance (i.e., lower switch costs) in the preHD-B group. No correlations were present within the preHD-A group.

4. Discussion

We investigated *cross-sectional* and *longitudinal* differences in regional and global topological properties between subjects with premanifest and early manifest HD and healthy controls. In this first-of-its-kind analysis in HD, we revealed both baseline and longitudinal changes in the connectome of premanifest gene carriers and subjects with early manifest disease. We also demonstrated correlations between graph metrics on one hand, and clinical and behavioural measures, on the other hand. These results provide novel insights into the dynamics of brain neuropathology occurring in HD and the relationships with commonly used neurocognitive measures.

4.1. Longitudinal decreases in network measures

The principal finding from this study was a significant reduction over time of nodal betweenness centrality both in the early manifest HD and preHD-B groups within the 2 year study period as compared to the preHD-A and control groups. The locations of these nodes included the left orbitofrontal cortex and left paracentral lobule. The reduction of betweenness centrality in these regions indicates that the shortest paths passing through these areas were reduced. This in turn implies a decrease of importance of these nodes to overall network integrity.

The orbitofrontal cortex is involved in decision making and cognitive and emotional processing [65]. Atrophy in this structure has been associated with impaired recognition of negative emotions in HD [66,67]. The paracentral lobule, a component of the sensorimotor system [68], has previously been implicated in HD where atrophy was also demonstrated [69]. The current results corroborate previous findings by demonstrating a longitudinal reduction in nodal betweenness centrality, suggesting a decreased capability of these nodes in facilitating communication between different brain regions in HD.

In the combined preHD group, a significant reduction over time of the clustering coefficient was also shown in the left medial prefrontal cortex when compared to healthy controls. This finding implies a decrease of functional segregation in this node. In other words, the left

Fig. 6. Correlations between changes in network parameters, and changes in clinical and neurocognitive functioning.

stage of the disease, intervention could be aimed at preserving this brain organization associated with health, especially because of the presumed degradation of this network quality in advanced stages of the disease. Such a disruption in later stages of HD is yet to be established, though studies into different disorders affecting the brain have revealed disruptions in the small-world topological organization [19,29]. The results presented here imply that, at least at the preHD and early manifest stages of HD, there is no evidence for a 'disconnection syndrome' from a network perspective. Studies in other neurological disorders, such as multiple sclerosis [24,25], Alzheimer's disease (reviewed [73]), schizophrenia [29] and traumatic brain injury [27] have found support for such a pathological model. The lack of this finding in this study is encouraging, as preservation of normal brain network architecture through intervention might be used as a secondary outcome for maintaining efficient brain function. It should be clear, though, that such a secondary outcome should be coupled with cognitive assessments given the intricate relationship between brain structure and function.

4.3. Making 'real-world' sense of network measures

Providing a translation from network measures to cognitive function and clinical state not only validates these measures, but also indicates possible usability in biomarker research. Interesting baseline correlations between graph metrics and neurocognitive measures were present in the preHD group. Specifically an inverse relationship between the switch cost of the TMT, regarded as a measure of cognitive flexibility, and clustering coefficient and local efficiency was found. These findings suggest that higher switching costs are associated with a loss in capability of processing information from a local network perspective. In the preHD-B group only, a positive correlation was observed between performance on SWR and global efficiency. This suggests that, in line with expectations, increases in the efficiency with which information can be transmitted globally are linked to higher processing speed.

Longitudinally, an increase in the UHDRS-TMS was negatively associated with small-worldness in the early manifest HD group, indicating that a decrease in 'wiring-efficiency' was related to an increase in motor score. The association found between increases on the reported symptoms on BDI-II and decreases in normalized path length in the preHD group provides evidence for coupled decreases in global integration with increases in depression scores. In the preHD-B group, we found that longitudinal increases in the switch cost of the TMT were correlated with longitudinal decreases in the clustering coefficient, again pointing to an association between this cognitive measure and local network properties.

4.4. Changing landscapes of hubs

Hubs are considered essential regions for coordinating brain functions, playing a central role in network resilience to brain injury [48, 74]. The dynamic nature of hub-status found in this study could prove informative in understanding the nature of disease progression and compensatory mechanisms at play in (pre) HD as reflected by the temporal relation between hub-status loss and gain. A highlight from our findings in this context was the hub-status gain found in preHD in the right superior parietal gyrus in the second visit. Using functional MRI, this region has been shown to play a compensatory role in maintaining normal motor function in preHD [75,76]. Although admittedly speculative at this stage, this finding could be attributed to an increased need for compensation with progression of neurodegeneration in time, making a reorganization of coordinating brain regions necessary for maintaining normal motor function. Another interesting finding was the contrast of hub-status gain for the right medial part of the superior frontal gyrus in early manifest HD compared to the loss of this status in the preHD group in the second visit. This type of information could further our understanding of compensatory mechanisms at play maintaining

medial prefrontal cortex seems to become less densely interconnected with surrounding nodes over time, suggesting a local reduction of internodal processing of information. The medial prefrontal cortex is a region involved in planning and problem solving [70], where in a previous study in preHD a lower functional connectivity has been demonstrated [71]. Moreover, a functional MRI study in preHD and manifest HD revealed reduced connectivity of the medial prefrontal cortex, representing a functional correlate of impaired executive function [72]. Therefore, in our opinion, this is an important finding potentially providing a structural explanation for the dynamics of observed reductions in higher cognitive abilities occurring in gene carriers prior to manifestation of motor signs.

4.2. Preserved small-world organization in early HD

Another important finding is the preserved small-world organization within preHD and early manifest HD compared to healthy controls. With this finding in mind, we suggest that also in the early manifest

seemingly normal brain function in the premanifest stage of the disease, despite clear evidence of neurodegeneration provided by independent imaging studies even more than a decade prior to expected disease onset [2,77].

4.5. Strengths and limitations

Strengths of this study include a standardized scan protocol with high-quality diffusion MRI data on two time points with assessments of multiple neurocognitive domains in a well described population from the TRACK-HD study. Moreover, in this study we have reconstructed the anatomical networks with constrained spherical deconvolution tractography, which in contrast to diffusion tensor imaging based tractography has the advantage of taking fibre crossings into account [9,41,78].

There are several limitations in the methods being applied in the present study, such as the used parcellation scheme for defining the network nodes for the graph theoretical analysis. Multimodal integration of in- and ex-vivo data into a probabilistic atlas [79] may offer a better biologically principled approach as a parcellation scheme than the AAL atlas used in this study. Furthermore, while reproducibility studies have often demonstrated good or excellent intraclass correlation coefficient (ICC) measurements variance (for a recent review [80]), more studies measuring the test–retest reliability of graph metrics of structural networks are needed.

Moreover, the number of reconstructed fibres was used to weight the edges in the calculation of the connection matrix and consequently the network measures. Although other indices of white matter organization, such as fractional anisotropy, mean diffusivity, and level of myelination, have previously been applied to define the connectivity matrices (e.g., [81,82]), there is currently no consensus on the optimal weighting method in terms of sensitivity and specificity to pathological effects.

5. Conclusions

This is the first study providing insights into longitudinal structural correlates with clinical state and cognitive function from a network perspective in HD. Strengthened by significant correlations with clinical and cognitive deficits, dynamics of the connectome, in the form of decreases of global and/or local efficiencies, were present in both the premanifest and early manifest stages of the disease. Furthermore, a changing hub landscape was demonstrated, contributing to our increased understanding of potential compensatory mechanisms at play, especially in preHD. The study further demonstrates preserved efficient dynamics of brain networks the premanifest and early manifest stages of the disease. We conclude that assessing the connectome provides not only a novel approach with a biomarker potential in HD, but also potential new insights into compensatory strategies of the brain in neurodegenerative disorders.

Acknowledgments

Appendix A. Supplementary data

Supplementary material for this article can be found online at http://dx.doi.org/10.1016/j.nicl.2015.07.003.

References

The Huntington's Disease Collaborative Research Group, 1993. A novel gene containing a trinucleotide repeat that is expanded and unstable on Huntington's disease chromosomes. Cell 72 (6), 971–983. http://dx.doi.org/10.1016/0092-8674(93)90585-E8458085.

Tabrizi, S.J., Langbehn, D.R., Leavitt, B.R., Roos, R.A., Durr, A., Craufurd, D., Kennard, C., Hicks, S.L., Fox, N.C., Scahill, R.I., Borowsky, B., Tobin, A.J., Rosas, H.D., Johnson, H., Reilmann, R., Landwehrmeyer, B., Stout, J.C., TRACK-HD investigators, 2009. Biological and clinical manifestations of Huntington's disease in the longitudinal TRACK-HD study: cross-sectional analysis of baseline data. Lancet Neurol. 8 (9), 791–801. http://dx.doi.org/10.1016/S1474-4422(09)70170-X19646924.

Aylward, E.H., Liu, D., Nopoulos, P.C., Ross, C.A., Pierson, R.K., Mills, J.A., Long, J.D., Paulsen, J.S., PREDICT-HD Investigators and Coordinators of the Huntington Study Group, 2012. Striatal volume contributes to the prediction of onset of Huntington disease in incident cases. Biol. Psychiatry 71 (9), 822–828. http://dx.doi.org/10.1016/j.biopsych.2011.07.03021907324.

Hadzi, T.C., Hendricks, A.E., Latourelle, J.C., Lunetta, K.L., Cupples, L.A., Gillis, T., Mysore, J.S., Gusella, J.F., MacDonald, M.E., Myers, R.H., Vonsattel, J.P., 2012. Assessment of cortical and striatal involvement in 523 Huntington disease brains. Neurology 79 (16), 1708–1715. http://dx.doi.org/10.1212/WNL.0b013e31826e9a5d23035064.

Sánchez-Castañeda, C., Squitieri, F., Di Paola, M., Dayan, M., Petrollini, M., Sabatini, U., 2015. The role of iron in gray matter degeneration in Huntington's disease: a magnetic resonance imaging study. Hum. Brain Mapp. 36 (1), 50–66. http://dx.doi.org/10.1002/hbm.2261225145324.

Basser, P.J., Mattiello, J., LeBihan, D., 1994. MR diffusion tensor spectroscopy and imaging. Biophys. J. 66 (1), 259–267. http://dx.doi.org/10.1016/S0006-3495(94)80775-18130344.

Pierpaoli, C., Jezzard, P., Basser, P.J., Barnett, A., Di Chiro, G., 1996. Diffusion tensor MR imaging of the human brain. Radiology 201 (3), 637–648. http://dx.doi.org/10.1148/radiology.201.3.89392098939209.

Jones, D.K., Leemans, A., 2011. Diffusion tensor imaging. Methods Mol. Biol. 711, 127–144. http://dx.doi.org/10.1007/978-1-61737-992-5_621279600.

Tournier, J.D., Mori, S., Leemans, A., 2011. Diffusion tensor imaging and beyond. Magn. Reson. Med. 65 (6), 1532–1556. http://dx.doi.org/10.1002/mrm.2292421469191.

Della Nave, R., Ginestroni, A., Tessa, C., Giannelli, M., Piacentini, S., Filippi, M., Mascalchi, M., 2010. Regional distribution and clinical correlates of white matter structural damage in Huntington disease: a tract-based spatial statistics study. A.J.N.R. Am. J. Neuroradiol. 31 (9), 1675–1681. http://dx.doi.org/10.3174/ajnr.A212820488902.

Bohanna, I., Georgiou-Karistianis, N., Sritharan, A., Asadi, H., Johnston, L., Churchyard, A., Egan, G., 2011. Diffusion tensor imaging in Huntington's disease reveals distinct patterns of white matter degeneration associated with motor and cognitive deficits. Brain Imaging Behav. 5 (3), 171–180. http://dx.doi.org/10.1007/s11682-011-9121-821437574.

Dumas, E.M., van den Bogaard, S.J., Ruber, M.E., Reilman, R.R., Stout, J.C., Craufurd, D., Hicks, S.L., Kennard, C., Tabrizi, S.J., van Buchem, M.A., van der Grond, J., Roos, R.A., 2012. Early changes in white matter pathways of the sensorimotor cortex in premanifest Huntington's disease. Hum. Brain Mapp. 33 (1), 203–212. http://dx.doi.org/10.1002/hbm.2120521264990.

Hobbs, N.Z., Cole, J.H., Farmer, R.E., Rees, E.M., Crawford, H.E., Malone, I.B., Roos, R.A., Sprengelmeyer, R., Durr, A., Landwehrmeyer, B., Scahill, R.I., Tabrizi, S.J., Frost, C., 2012. Evaluation of multi-modal, multi-site neuroimaging measures in Huntington's disease: baseline results from the Paddington study. Neuroimage Clin. 2, 204–211. http://dx.doi.org/10.1016/j.nicl.2012.12.00124179770.

Phillips, O., Squitieri, F., Sanchez-Castaneda, C., Elifani, F., Caltagirone, C., Sabatini, U., Di Paola, M., 2014. Deep white matter in Huntington's disease. PLOS One 9 (10). http://dx.doi.org/10.1371/journal.pone.010967625340651.

Vandenberghe, W., Demaerel, P., Dom, R., Maes, F., 2009. Diffusion-weighted versus volumetric imaging of the striatum in early symptomatic Huntington disease. J. Neurol. 256 (1), 109–114. http://dx.doi.org/10.1007/s00415-009-0086-019267169.

Weaver, K.E., Richards, T.L., Liang, O., Laurino, M.Y., Samii, A., Aylward, E.H., 2009. Longitudinal diffusion tensor imaging in Huntington's disease. Exp. Neurol. 216 (2), 525–529. http://dx.doi.org/10.1016/j.expneurol.2008.12.02619320010.

Sritharan, A., Egan, G.F., Johnston, L., Horne, M., Bradshaw, J.L., Bohanna, I., Asadi, H., Cunnington, R., Churchyard, A.J., Chua, P., Farrow, M., Georgiou-Karistianis, N., 2010. A longitudinal diffusion tensor imaging study in symptomatic Huntington's disease. J. Neurol. Neurosurg. Psychiatry 81 (3), 257–262. http://dx.doi.org/10.1136/jnnp.2007.14278619237387.

Bach, M., Laun, F.B., Leemans, A., Tax, C.M., Biessels, G.J., Stieltjes, B., Maier-Hein, K.H., 2014. Methodological considerations on tract-based spatial statistics (TBSS). Neuroimage 100, 358–369. http://dx.doi.org/10.1016/j.neuroimage.2014.06.02124945661.

He, Y., Chen, Z., Evans, A., 2008. Structural insights into aberrant topological patterns of large-scale cortical networks in Alzheimer's disease. J. Neurosci. 28 (18), 4756–4766. http://dx.doi.org/10.1523/JNEUROSCI.0141-08.200818448652.

Supekar, K., Menon, V., Rubin, D., Musen, M., Greicius, M.D., 2008. Network analysis of intrinsic functional brain connectivity in Alzheimer's disease. PLOS Comput. Biol. 4 (6). http://dx.doi.org/10.1371/journal.pcbi.100010018584043.

Lo, C.Y., Wang, P.N., Chou, K.H., Wang, J., He, Y., Lin, C.P., 2010. Diffusion tensor tractography reveals abnormal topological organization in structural cortical networks in Alzheimer's disease. J. Neurosci. 30 (50), 16876–16885. http://dx.doi.org/10.1523/JNEUROSCI.4136-10.201021159959.

Reijmer, Y.D., Leemans, A., Caeyenberghs, K., Heringa, S.M., Koek, H.L., Biessels, G.J., Utrecht Vascular Cognitive Impairment Study Group, 2013. Disruption of cerebral networks and cognitive impairment in Alzheimer disease. Neurology 80 (15), 1370–1377. http://dx.doi.org/10.1212/WNL.0b013e31828c2ee523486876.

Heringa, S.M., Reijmer, Y.D., Leemans, A., Koek, H.L., Kappelle, L.J., Biessels, G.J., Utrecht Vascular Cognitive Impairment (VCI) Study Group, 2014. Multiple microbleeds are related to cerebral network disruptions in patients with early Alzheimer's disease. J. Alzheimers Dis. 38 (1), 211–221. http://dx.doi.org/10.3233/JAD-13054223948936.

He, Y., Dagher, A., Chen, Z., Charil, A., Zijdenbos, A., Worsley, K., Evans, A., 2009. Impaired small-world efficiency in structural cortical networks in multiple sclerosis associated with white matter lesion load. Brain 132 (12), 3366–3379. http://dx.doi.org/10.1093/brain/awp08919439423.

Shu, N., Liu, Y., Li, K., Duan, Y., Wang, J., Yu, C., Dong, H., Ye, J., He, Y., 2011. Diffusion tensor tractography reveals disrupted topological efficiency in white matter structural networks in multiple sclerosis. Cereb. Cortex 21 (11), 2565–2577. http://dx.doi.org/10.1093/cercor/bhr03921467209.

Caeyenberghs, K., Leemans, A., Heitger, M.H., Leunissen, I., Dhollander, T., Sunaert, S., Dupont, P., Swinnen, S.P., 2012. Graph analysis of functional brain networks for cognitive control of action in traumatic brain injury. Brain 135 (4), 1293–1307. http://dx.doi.org/10.1093/brain/aws04822427332.

Caeyenberghs, K., Leemans, A., Leunissen, I., Gooijers, J., Michiels, K., Sunaert, S., Swinnen, S.P., 2014. Altered structural networks and executive deficits in traumatic brain injury patients. Brain Struct. Funct. 219 (1), 193–209. http://dx.doi.org/10.1007/s00429-012-0494-223232826.

Bassett, D.S., Bullmore, E., Verchinski, B.A., Mattay, V.S., Weinberger, D.R., Meyer-Lindenberg, A., 2008. Hierarchical organization of human cortical networks in health and schizophrenia. J. Neurosci. 28 (37), 9239–9248. http://dx.doi.org/10.1523/JNEUROSCI.1929-08.200818784304.

Liu, Y., Liang, M., Zhou, Y., He, Y., Hao, Y., Song, M., Yu, C., Liu, H., Liu, Z., Jiang, T., 2008. Disrupted small-world networks in schizophrenia. Brain 131 (4), 945–961. http://dx.doi.org/10.1093/brain/awn01818299296.

Poudel, G.R., Stout, J.C., Domínguez D, J.F., Salmon, L., Churchyard, A., Chua, P., Georgiou-Karistianis, N., Egan, G.F., 2014. White matter connectivity reflects clinical and cognitive status in Huntington's disease. Neurobiol. Dis. 65, 180–187. http://dx.doi.org/10.1016/j.nbd.2014.01.01324480090.

Tabrizi, S.J., Scahill, R.I., Durr, A., Roos, R.A., Leavitt, B.R., Jones, R., Landwehrmeyer, G.B., Fox, N.C., Johnson, H., Hicks, S.L., Kennard, C., Craufurd, D., Frost, C., Langbehn, D.R., Reilmann, R., Stout, J.C., TRACK-HD Investigators, 2011. Biological and clinical changes in premanifest and early stage Huntington's disease in the TRACK-HD study: the 12-month longitudinal analysis. Lancet Neurol. 10 (1), 31–42. http://dx.doi.org/10.1016/S1474-4422(10)70276-321130037.

Langbehn, D.R., Brinkman, R.R., Falush, D., Paulsen, J.S., Hayden, M.R., International Huntington's Disease Collaborative Group, 2004. A new model for prediction of the age of onset and penetrance for Huntington's disease based on CAG length. Clin. Genet. 65 (4), 267–277. http://dx.doi.org/10.1111/j.1399-0004.2004.00241.x15025718.

Penney Jr., J.B., Vonsattel, J.P., MacDonald, M.E., Gusella, J.F., Myers, R.H., 1997. CAG repeat number governs the development rate of pathology in Huntington's disease. Ann. Neurol. 41 (5), 689–692. http://dx.doi.org/10.1002/ana.4104105219153534.

O'Rourke, J.J., Beglinger, L.J., Smith, M.M., Mills, J., Moser, D.J., Rowe, K.C., Langbehn, D.R., Duff, K., Stout, J.C., Harrington, D.L., Carlozzi, N., Paulsen, J.S., 2011. The trail making test in prodromal Huntington disease: contributions of disease progression to test performance. J. Clin. Exp. Neuropsychol. 33 (5), 567–579. http://dx.doi.org/10.1080/13803395.2010.54122821302170.

Delmaire, C., Dumas, E.M., Sharman, M.A., van den Bogaard, S.J., Valabregue, R., Jauffret, C., Justo, D., Reilmann, R., Stout, J.C., Craufurd, D., Tabrizi, S.J., Roos, R.A., Durr, A., Lehéricy, S., 2013. The structural correlates of functional deficits in early Huntington's disease. Hum. Brain Mapp. 34 (9), 2141–2153. http://dx.doi.org/10.1002/hbm.2205522438242.

Schmand, B., Bakker, D., Saan, R., Louman, J., 1991. [The Dutch Reading Test for Adults: a measure of premorbid intelligence level]. Tijdschr. Gerontol. Geriatr. 22 (1), 15–191877068.

Leemans, A., Jeurissen, B., Sijbers, J., Jones, D.K., 2009. Explore DTI: a graphical toolbox for processing, analyzing, and visualizing diffusion MR data. 17th Annual Meeting of Intl Soc. Mag. Reson. Med, Hawaii, USA, p. 3537.

Irfanoglu, M.O., Walker, L., Sarlls, J., Marenco, S., Pierpaoli, C., 2012. Effects of image distortions originating from susceptibility variations and concomitant fields on diffusion MRI tractography results. Neuroimage 61 (1), 275–288. http://dx.doi.org/10.1016/j.neuroimage.2012.02.05422401760.

Veraart, J., Sijbers, J., Sunaert, S., Leemans, A., Jeurissen, B., 2013. Weighted linear least squares estimation of diffusion MRI parameters: strengths, limitations, and pitfalls. Neuroimage 81, 335–346. http://dx.doi.org/10.1016/j.neuroimage.2013.05.02823684865.

Tax, C.M., Otte, W.M., Viergever, M.A., Dijkhuizen, R.M., Leemans, A., 2015. REKINDLE: robust extraction of kurtosis INDices with linear estimation. Magn. Reson. Med. 73 (2), 794–808. http://dx.doi.org/10.1002/mrm.2516524687400.

Tournier, J.D., Calamante, F., Connelly, A., 2007. Robust determination of the fibre orientation distribution in diffusion MRI: non-negativity constrained super-resolved spherical deconvolution. Neuroimage 35 (4), 1459–1472. http://dx.doi.org/10.1016/j.neuroimage.2007.02.01617379540.

Jeurissen, B., Leemans, A., Jones, D.K., Tournier, J.D., Sijbers, J., 2011. Probabilistic fiber tracking using the residual bootstrap with constrained spherical deconvolution. Hum. Brain Mapp. 32 (3), 461–479. http://dx.doi.org/10.1002/hbm.2103221319270.

Tax, C.M., Jeurissen, B., Vos, S.B., Viergever, M.A., Leemans, A., 2014. Recursive calibration of the fiber response function for spherical deconvolution of diffusion MRI data. Neuroimage 86, 67–80. http://dx.doi.org/10.1016/j.neuroimage.2013.07.06723927905.

Tzourio-Mazoyer, N., Landeau, B., Papathanassiou, D., Crivello, F., Etard, O., Delcroix, N., Mazoyer, B., Joliot, M., 2002. Automated anatomical labeling of activations in SPM using a macroscopic anatomical parcellation of the MNI MRI single-subject brain. Neuroimage 15 (1), 273–289. http://dx.doi.org/10.1006/nimg.2001.097811771995.

Klein, S., Staring, M., Murphy, K., Viergever, M.A., Pluim, J.P., 2010. Elastix: a toolbox for intensity-based medical image registration. I.E.E.E. Trans. Med. Imaging 29 (1), 196–205. http://dx.doi.org/10.1109/TMI.2009.203561619923044.

De Groot, M., Vernooij, M.W., Klein, S., Ikram, M.A., Vos, F.M., Smith, S.M., Niessen, W.J., Andersson, J.L., 2013. Improving alignment in tract-based spatial statistics: evaluation and optimization of image registration. Neuroimage 76, 400–411. http://dx.doi.org/10.1016/j.neuroimage.2013.03.01523523807.

Li, Y., Liu, Y., Li, J., Qin, W., Li, K., Yu, C., Jiang, T., 2009. Brain anatomical network and intelligence. PLOS Comput. Biol. 5 (5). http://dx.doi.org/10.1371/journal.pcbi.100039519492086.

Rubinov, M., Sporns, O., 2010. Complex network measures of brain connectivity: uses and interpretations. Neuroimage 52 (3), 1059–1069. http://dx.doi.org/10.1016/j.neuroimage.2009.10.00319819337.

Hosseini, S.M., Hoeft, F., Kesler, S.R., 2012. GAT: a graph-theoretical analysis toolbox for analyzing between-group differences in large-scale structural and functional brain networks. PLOS One 7 (7), e40709. http://dx.doi.org/10.1371/journal.pone.004070922808240.

Hosseini, S.M., Koovakkattu, D., Kesler, S.R., 2012. Altered small-world properties of gray matter networks in breast cancer. B.M.C. Neurol. 12, 28. http://dx.doi.org/10.1186/1471-2377-12-2822632066.

Hosseini, S.M., Black, J.M., Soriano, T., Bugescu, N., Martinez, R., Raman, M.M., Kesler, S.R., Hoeft, F., 2013. Topological properties of large-scale structural brain networks in children with familial risk for reading difficulties. Neuroimage 71, 260–274. http://dx.doi.org/10.1016/j.neuroimage.2013.01.01323333415.

Van Wijk, B.C., Stam, C.J., Daffertshofer, A., 2010. Comparing brain networks of different size and connectivity density using graph theory. PLOS One 5 (10), e13701. http://dx.doi.org/10.1371/journal.pone.001370121060892.

Latora, V., Marchiori, M., 2001. Efficient behavior of small-world networks. Phys. Rev. Lett. 87 (19), 198701. http://dx.doi.org/10.1103/PhysRevLett.87.19870111690461.

Sporns, O., Zwi, J.D., 2004. The small world of the cerebral cortex. Neuroinformatics 2 (2), 145–162. http://dx.doi.org/10.1385/NI:2:2:14515319512.

Onnela, J.P., Saramäki, J., Kertész, J., Kaski, K., 2005. Intensity and coherence of motifs in weighted complex networks. Phys. Rev. E Stat. Nonlin. Soft Matter Phys. 71 (6 Pt 2), 065103. http://dx.doi.org/10.1103/PhysRevE.71.06510316089800.

Opsahl, T., Panzarasa, P., 2009. Clustering in weighted networks. Soc. Netw. 31 (2), 155–163. http://dx.doi.org/10.1016/j.socnet.2009.02.002.

Maslov, S., Sneppen, K., 2002. Specificity and stability in topology of protein networks. Science 296 (5569), 910–913. http://dx.doi.org/10.1126/science.106510311988575.

Hosseini, S.M., Kesler, S.R., 2013. Influence of choice of null network on small-world parameters of structural correlation networks. PLOS One 8 (6), e67354. http://dx.doi.org/10.1371/journal.pone.006735423840672.

Watts, D.J., Strogatz, S.H., 1998. Collective dynamics of 'small-world' networks. Nature 393 (6684), 440–442. http://dx.doi.org/10.1038/309189623998.

Humphries, M.D., Gurney, K., 2008. Network 'small-world-ness': a quantitative method for determining canonical network equivalence. PLOS One 3 (4). http://dx.doi.org/10.1371/journal.pone.000205118446219.

Bassett, D.S., Bullmore, E., 2006. Small-world brain networks. Neuroscientist 12 (6), 512–523. http://dx.doi.org/10.1177/107385840629318217079517.

Freeman, L.C., 1978. Centrality in social networks conceptual clarification. Soc. Netw. 1 (3), 215–239. http://dx.doi.org/10.1016/0378-8733(78)90021-7.

Kesler, S.R., Wefel, J.S., Hosseini, S.M.H., Cheung, M., Watson, C.L., Hoeft, F., 2013. Default mode network connectivity distinguishes chemotherapy-treated breast cancer survivors from controls. Proc. Natl. Acad. Sci. U. S. A. 110 (28), 11600–11605. http://dx.doi.org/10.1073/pnas.121455111023798392.

Genovese, C.R., Lazar, N.A., Nichols, T., 2002. Thresholding of statistical maps in functional neuroimaging using the false discovery rate. Neuroimage 15 (4), 870–878. http://dx.doi.org/10.1006/nimg.2001.103711906227.

Kringelbach, M.L., Rolls, E.T., 2004. The functional neuroanatomy of the human orbitofrontal cortex: evidence from neuroimaging and neuropsychology. Prog. Neurobiol. 72 (5), 341–372. http://dx.doi.org/10.1016/j.pneurobio.2004.03.00615157726.

Henley, S.M., Wild, E.J., Hobbs, N.Z., Warren, J.D., Frost, C., Scahill, R.I., Ridgway, G.R., MacManus, D.G., Barker, R.A., Fox, N.C., Tabrizi, S.J., 2008. Defective emotion recognition in early HD is neuropsychologically and anatomically generic. Neuropsychologia 46 (8), 2152–2160. http://dx.doi.org/10.1016/j.neuropsychologia.2008.02.02518407301.

Ille, R., Schäfer, A., Scharmüller, W., Enzinger, C., Schöggl, H., Kapfhammer, H.P., Schienle, A., 2011. Emotion recognition and experience in Huntington disease: a voxel-based morphometry study. J. Psychiatry Neurosci. 36 (6), 383–390. http://dx.doi.org/10.1503/jpn.10014321406159.

White, L.E., Andrews, T.J., Hulette, C., Richards, A., Groelle, M., Paydarfar, J., Purves, D., 1997. Structure of the human sensorimotor system. I: Morphology and cytoarchitecture of the central sulcus. Cereb. Cortex 7 (1), 18–30. http://dx.doi.org/10.1093/cercor/7.1.189023429.

Kassubek, J., Juengling, F.D., Kioschies, T., Henkel, K., Karitzky, J., Kramer, B., et al., 2004. Topography of cerebral atrophy in early Huntington's disease: a voxel based morphometric MRI study. J. Neurol. Neurosurg. Psychiatry 75 (2), 213–22014742591.

Alvarez, J.A., Emory, E., 2006. Executive function and the frontal lobes: a meta-analytic review. Neuropsychol. Rev. 16 (1), 17–42. http://dx.doi.org/10.1007/s11065-006-9002-x16794878.

Wolf, R.C., Sambataro, F., Vasic, N., Wolf, N.D., Thomann, P.A., Saft, C., Landwehrmeyer, G.B., Orth, M., 2012. Default-mode network changes in preclinical Huntington's disease. Exp. Neurol. 237 (1), 191–198. http://dx.doi.org/10.1016/j.expneurol.2012.06.01422742947.

Unschuld, P.G., Liu, X., Shanahan, M., Margolis, R.L., Bassett, S.S., Brandt, J., Schretlen, D.J., Redgrave, G.W., Hua, J., Hock, C., Reading, S.A., van Zijl, P.C., Pekar, J.J., Ross, C.A., 2013. Prefrontal executive function associated coupling relates to Huntington's disease stage. Cortex 49 (10), 2661–2673. http://dx.doi.org/10.1016/j.cortex.2013.05.01523906595.

Xie, T., He, Y., 2011. Mapping the Alzheimer's brain with connectomics. Front. Psychiatry 2, 77. http://dx.doi.org/10.3389/fpsyt.2011.0007722291664.

Cole, M.W., Pathak, S., Schneider, W., 2010. Identifying the brain's most globally connected regions. Neuroimage 49 (4), 3132–3148. http://dx.doi.org/10.1016/j.neuroimage.2009.11.00119909818.

Klöppel, S., Draganski, B., Siebner, H.R., Tabrizi, S.J., Weiller, C., Frackowiak, R.S., 2009. Functional compensation of motor function in pre-symptomatic Huntington's disease. Brain 132 (6), 1624–1632. http://dx.doi.org/10.1093/brain/awp08119369489.

Scheller, E., Abdulkadir, A., Peter, J., Tabrizi, S.J., Frackowiak, R.S., Klöppel, S., 2013. Interregional compensatory mechanisms of motor functioning in progressing preclinical neurodegeneration. Neuroimage 75, 146–154. http://dx.doi.org/10.1016/j.neuroimage.2013.02.05823501047.

Paulsen, J.S., Nopoulos, P.C., Aylward, E., Ross, C.A., Johnson, H., Magnotta, V.A., Juhl, A., Pierson, R.K., Mills, J., Langbehn, D., Nance, M., PREDICT-HD Investigators and Coordinators of the Huntington's Study Group (HSG), 2010. Striatal and white matter predictors of estimated diagnosis for Huntington disease. Brain Res. Bull. 82 (3–4), 201–207. http://dx.doi.org/10.1016/j.brainresbull.2010.04.00320385209.

Jeurissen, B., Leemans, A., Tournier, J.D., Jones, D.K., Sijbers, J., 2013. Investigating the prevalence of complex fiber configurations in white matter tissue with diffusion magnetic resonance imaging. Hum. Brain Mapp. 34 (11), 2747–2766. http://dx.doi.org/10.1002/hbm.2209922611035.

Eickhoff, S.B., Stephan, K.E., Mohlberg, H., Grefkes, C., Fink, G.R., Amunts, K., Zilles, K., 2005. A new SPM toolbox for combining probabilistic cytoarchitectonic maps and functional imaging data. Neuroimage 25 (4), 1325–1335. http://dx.doi.org/10.1016/j.neuroimage.2004.12.03415850749.

Welton, T., Kent, D.A., Auer, D.P., Dineen, R.A., 2015. Reproducibility of graph-theoretic brain network metrics: a systematic review. Brain Connectivity 5 (4), 193–202. http://dx.doi.org/10.1089/brain.2014.031325490902.

Gong, G., He, Y., Concha, L., Lebel, C., Gross, D.W., Evans, A.C., Beaulieu, C., 2009. Mapping anatomical connectivity patterns of human cerebral cortex using in vivo diffusion tensor imaging tractography. Cereb. Cortex 19 (3), 524–536. http://dx.doi.org/10.1093/cercor/bhn10218567609.

Van den Heuvel, M.P., Mandl, R.C., Stam, C.J., Kahn, R.S., Hulshoff Pol, H.E., 2010. Aberrant frontal and temporal complex network structure in schizophrenia: a graph theoretical analysis. J. Neurosci. 30 (47), 15915–15926. http://dx.doi.org/10.1523/JNEUROSCI.2874-10.201021106830.